Full Length Article

High pressure sorption of various hydrocarbons and carbon dioxide in Kimmeridge Blackstone and isolated kerogen

Huangjing Zhao, Tianhao Wu, Abbas Firoozabadi*

Reservoir Engineering Research Institute, 595 Lytton Avenue Suite B, Palo Alto, CA 94301, USA

ABSTRACT

We have measured adsorption and desorption of methane, ethane, propane, *n*-butane, *iso*-butane and carbon dioxide in Kimmeridge Blackstone at high pressures at temperatures of 60, 90 and 120 °C. Sorption of various light hydrocarbons and carbon dioxide in the isolated kerogen at 60 °C was also investigated. In our measurements, we used the gravimetric method. Physical and chemical properties of samples were measured to provide insight into sorption. Methane, ethane and carbon dioxide sorption was measured to 150 bar. Due to low vapor pressure of propane at 60 and 90 °C, the sorption was measured to 15 bar at 60 °C and 30 bar at 90 °C, respectively. At 120 °C, propane sorption was measured to 30 bar. Similarly, *n*-butane and *iso*-butane sorption was studied to 5, 9.5 and 15 bar at 60, 90 and 120 °C, respectively. Compared to sorption of these gases at moderate pressure in our recent work, high pressure sorption shows more pronounced hysteresis and non-monotonic excess sorption. In this work, we use the adsorbed layer density, estimated from grand canonical Monte Carlo (GCMC) simulations, and the liquid density to compute the absolute adsorption and examine the difference between the two. The results show that the absolute adsorption estimated with the two densities is significantly different in methane but similar in the other species. The butanes, *n*-butane and *iso*-butane, despite close bulk densities have very different adsorption. The adsorbed layer densities by GCMC simulations are different by about 10% which partly account for the adsorption difference. Other mechanisms may be at play due to different shape of the two molecules.

1. Introduction

The Kimmeridge Blackstone, also known as Kimmeridge Clay oil shale, has been known since the Iron Age and used as a local coal substitute and heat source [1]. Kimmeridge Blackstone is an organic-rich sedimentary rock. A small amount of its organic matter such as bitumen can be extracted by organic solvents. However, most of the organic matters are insoluble complex organic compounds, known as kerogen. Kerogen is the predominant organic matter in most shales [2]. Generally, higher content of organic matter gives higher sorption of hydrocarbons and carbon dioxide. The inorganic part of Kimmeridge Blackstone has similarities to conventional formations and contains clay, calcite, quartz, etc.

Like other shales, an important feature of Kimmeridge Blackstone is the nanoscale size of pores, in both organic and inorganic matter. Adsorption of fluid species onto the inner surface of pores may contribute significantly to total fluid-in-place when the ratio of surface area to the pore volume increases [3,4]. Due to the nanoscale pores in shale, adsorption can be an important part of total species-in-place. Fluid-in-place may be divided by three categories: free molecules in the pores; adsorbed species onto the inner surfaces of the microscale and nanoscale pores; and dissolved species in the organic matter [5]. When there is fluid dissolution in organic matter of shale media, there may be swelling of the rock media.

Adsorption of methane and carbon dioxide in shale media has been studied by various authors. However, except in our recent work which reported adsorption and desorption of light hydrocarbons and carbon dioxide to moderate pressures [6], there is only one published report on ethane excess adsorption in shale. Gasparik et al. [7] have reported ethane excess adsorption in the Upper Chokier and Lower Toarcian shale rocks. They reported an inter-laboratory comparison of high pressure ethane adsorptions in two shale rack samples to 150 bar by gravimetric and manometric methods. The data were in terms of excess sorption based on zero adsorption volume and neglect of sample swelling. Except in our recent work, which was limited to moderate pressures [6] as mentioned above, to the best of our knowledge, there is no reported adsorption measurement of propane, *n*-butane, and *iso*-butane in the shale media. There is limited work on desorption of

---

methane and carbon dioxide in shale media, despite the fact that desorption is relevant in shale gas and oil production. Yuan et al. [8] have reported methane excess sorption in dry and moist shale samples from Sichuan Basin, China to 35 bar using a manometric method. They observed a slight hysteresis in dry shale and a strong hysteresis in moist shale. They plotted the computed absolute adsorption based on the assumption of constant adsorbed layer density for methane with the value of 0.421 g/mL which is close to the methane liquid density at the boiling point at atmospheric pressure. We will later discuss that the methane liquid density may not represent methane adsorption density.

We have reported adsorption and desorption of various light hydrocarbons and carbon dioxide in shales and isolated kerogens to a moderate pressure of 35 bar and lower and to a temperature 65 °C recently [6]. Theoretically, there should be no hysteresis in methane adsorption and desorption in mesoporous materials at reservoir temperatures [6]. However, we observed a measurable hysteresis in the methane and carbon dioxide sorption isotherms and a significant hysteresis in ethane, propane, and butane sorption isotherms in the whole pressure range. The hysteresis may be related to the reversible structure change during the sorption measurements [6]. Other possibilities include the location of adsorbed and desorbed molecules being different in different pores. A number of laboratory studies have reported methane and carbon dioxide sorption hysteresis in coal seams. The mechanism of hysteresis of methane and carbon dioxide in adsorption and desorption in coal is an open question, and many explanations have been proposed including moisture in the coal sample, surface geometry heterogeneity, chemical interaction, structural deformation, and insufficient waiting time [9]. For the heavier hydrocarbons, the capillary condensation causes the hysteresis, because the critical temperatures are close or even higher than reservoir temperature. If only the capillary condensation contributed to the hysteresis, the hysteresis may not cover the whole pressure range.

In this work, we investigate adsorption and desorption in Kimmeridge Blackstone and the isolated kerogen to 150 bar and to 120 °C for carbon dioxide, methane, and ethane. The pressure for other species was lower due to low vapor pressure, but all pressure limits were higher than our past work [6]. The Kimmeridge Blackstone has a very high kerogen content, which facilitates the investigation on the influence of kerogen in sorption. Through the grand canonical Monte Carlo (GCMC) simulations we compute the density of adsorbed layer to shed light on the effect of adsorbed layer density on absolute adsorption especially in relation to methane and *n*-butane and *iso*-butane. In methane, because of the large different temperature between the conditions of adsorption measurement and liquid density data, we may expect significant improvement based on GCMC simulation for the measured data interpretation. In *n*-butane and *iso*-butane, the bulk liquid densities are close but the adsorbed layer densities may be different. Adsorbed layer densities from molecular simulations are computed to shed light on the large adsorption difference between *n*-butane and *iso*-butane.

The remainder of this paper is organized as follows. First, the experimental methods of basic property measurements and adsorption and desorption measurements are introduced. The details of molecular simulations are also provided in this section. Second, the basic properties of the samples and the adsorption and desorption results of various hydrocarbons and carbon dioxide are presented. The difference of adsorption between *n*-butane and *iso*-butane is analyzed from the GCMC simulations. At the end, we present the key conclusions.

2. Experimental

2.1. Basic properties

Kimmeridge Blackstone from Blackstone band of Kimmeridge Clay from an outcrop at the east of Kimmeridge Bay in Dorset, UK was used to investigate adsorption and desorption. Large chunks of rock were

crushed first, and then grounded by a ball mill (Planetary Ball Mill PM 200, Retsch). The milled shale powder samples were dry sieved by a 200 mesh sieve (W.S. Tyler) to collect particles smaller than 75 μm for subsequent adsorption and desorption measurements. A Micromeritics Accelerated Surface Area and Porosimetry System (ASAP 2420) was used to determine the specific surface area and pore size distributions of the samples. A Thermo Scientific FLASH 2000 CHNS-O Analyzer was used for the elemental analysis, while total organic carbon content in the samples was analyzed by a CM150 Organic, Inorganic, and Total Carbon Analyzer (UIC, Inc.). The mineral composition of the samples (qualitative) was analyzed by a D8 ADVANCE X-ray Diffraction System (Bruker). The XRD quantitative mineralogy analysis and IR analysis were performed by Texray Laboratory Services, and the organic petrography (maceral) and thermal maturity (vitrinite reflectance) were analyzed by RPS Group. The quantitative XRD analyses of the samples were performed using a Bruker D5000 X-ray diffractometer with Cu Kα radiation source (λ = 1.5405 Å) and silicon drift detector. IR spectroscopy was performed by a Perkin Elmer Spectrum One FT-IR Spectrophotometer with an Attenuated Total Reflectance (ATR) attachment. For the organic petrography, the samples were investigated in white- and UV-light using a Zeiss Axio-Scope A1 at 625x (50x objective, and 1.25 optivar) in immersion oil. White- and UV-light was provided by an X-Cite 120 LED light source. Photographs were captured using a Gryphax camera attached to the Zeiss Axio-Scope A1, and Gryphax image-capture software. All images were then reproduced and enhanced in Microsoft Powerpoint software. A total of 300 counts of both organic and mineral matter were collected for each sample. The RPS methodology for vitrinite reflectance utilizes grey-scale technology that allows accurate measurement of small vitrinite particles, like those commonly encountered in shales and mudstones as dispersed organic matter. A minimum of 50 reflectance measurements were taken for each sample. High-resolution black and white photos were taken using a Gryphax digital camera, and grey-scale values measured using Zeiss AxioScope software. The grey-scale values were then translated into % Ro using a mathematical equation of grey-scale values calibrated to a vitrinite reflectance standard. A histogram of all values collected from a sample was then developed to identify the in-situ vitrinite data, and to subsequently calculate a definitive %Ro.

Kerogen was isolated from the Blackstone shale rock by acid treatment and Soxhlet extraction process [10]. Carbonates were removed by 6 N HCl acid at a temperature of around 60 °C. The remains were filtered and washed with deionized water (DI water) and oven-dried at 80 °C. Silicates were removed by a mixture of HCl and HF acids (6N HCl + 24 wt% HF) at around 60 °C, and the remains were filtered and washed with DI water and oven-dried again. Thereafter, Soxhlet extraction with toluene was used to remove extractable organic components. The treated samples were oven-dried under vacuum. All the chemicals used in this study were from Sigma-Aldrich.

2.2. Experimental set-up

Adsorption and desorption of methane (99.97%), ethane (99%), propane (99.5%), *n*-butane (99.999%) and *iso*-butane (99.999%), and carbon dioxide (99.5%) in the Blackstone shale rock and isolated kerogen were investigated using an ISOSORP® STATIC (SC-HP II) Automatic Gravimetric High Pressure Sorption Analyzer manufactured by RUBOTHERM. A high-pressure Isco syringe pump and a gas booster were used to charge the fluids to the machine. Methane, ethane, propane and carbon dioxide used in this study were from Praxair, Inc. *n*-butane and *iso*-butane (constant pressure cylinders, ~50 bar) were from Welker Engineered Products. Fig. 1 shows the schematic diagram of the gravimetric adsorption analyzer. The sorption is determined gravimetrically by weighing the sample using the patented magnetic suspension balance. The gas pressure in the instrument is controlled by a fully automatic pressure controller. Resolution of the magnetic suspension balance is 0.01 mg and the reproducibility is ± 0.04 mg
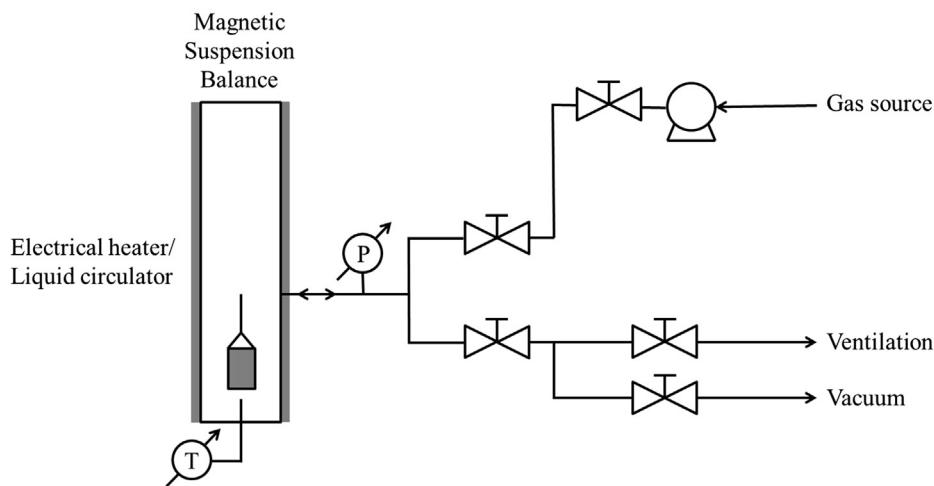
Fig. 1. Schematic diagram of the gravimetric gas adsorption analyzer.

Table 1
Basic mineralogy (wt%) of Kimmeridge Blackstone.

	Quartz	Feldspar	Calcite	Pyrite	Clay	Rest
Kimmeridge Blackstone	10	0	52	7	26	5

Table 3
CHNS-O composition and total organic carbon analysis of Blackstone and kerogen samples.

	H (wt%)	TC[1] (TOC[2]) (wt%)	N (wt%)	O (wt%)	S (wt%)	Rest (wt%)
Kimmeridge Blackstone	5.45	52.71 (51.19)	1.40	8.84	7.18	24.42
Kimmeridge kerogen	6.49	62.52 (62.52)	1.70	5.58	11.31	12.40

[1] TC: Total Carbon; [2]TOC: Total Organic Carbon.

Table 4
Petrographic components of Kimmeridge Blackstone (A total of 300 counts).

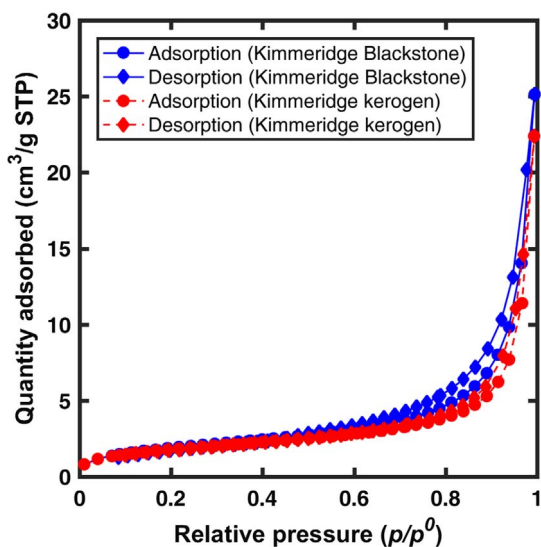|	Mineral Matter	Vitrinite	Inertinite	Liptinite
Kimmeridge Blackstone	115	8	3	174

Fig. 2. Nitrogen adsorption and desorption in Blackstone and kerogen powder samples at -195.85 °C.

Table 2
Surface area, average pore size and pore volume of Blackstone and kerogen powder samples.

	BET surface area (m²/g)	BJH pore volume (cm³/g)	BJH average pore size (nm)
Kimmeridge Blackstone	8.304	0.0336	18.5
Kimmeridge kerogen	6.568	0.0335	25.9

(standard deviation).

2.3. Experimental procedure

First, the weight (m^{SC}) and volume (V^{SC}) of the empty sample container were measured with helium gas (99.999%) at 60 °C. Starting from vacuum, the pressure was increased stepwise to 100 bar with helium gas. The decrease of the measured mass of the empty sample container with increasing pressure of the gas due buoyancy can used to determine the mass and volume of the sample container, m^{SC} and V^{SC}. This step is known as blank measurement. Next, around 1.0 to 1.2 g of sample was loaded to the sample container and was vacuum (ultimate vacuum with gas ballast is 0.01 mbar) dried at 200 °C until there was no weight change. This step is known as the sample pretreatment. In the third step, the weight (m^{S}) and the volume (V^{S}) of the loaded sample were determined with helium gas at 60 °C. V^{S} is the volume of the grain matrix and does not include the measured pore volume with Brunauer–Emmett–Teller (BET) model. Starting from vacuum, the pressure was increased stepwise to 100 bar with helium gas at a constant temperature. Based on the linear regression of the measured mass of the loaded sample versus increasing helium gas density, m^{S} and V^{S} were determined. This step is also known as buoyancy measurement. In the fourth step, the loaded shale sample was evacuated again at 200 °C until there was no weight change, and then the adsorption and desorption measurements were conducted. In the adsorption (desorption) measurement, the pressure of the gas was increased (decreased) stepwise at a constant temperature. After each adsorption/desorption measurement cycle, the loaded sample was regenerated by vacuum dry at 200 °C, followed by the next adsorption (desorption) measurement.

In the measurements, there are two forces acting on the sample, gravity force (F_A) and buoyancy force (F_B).

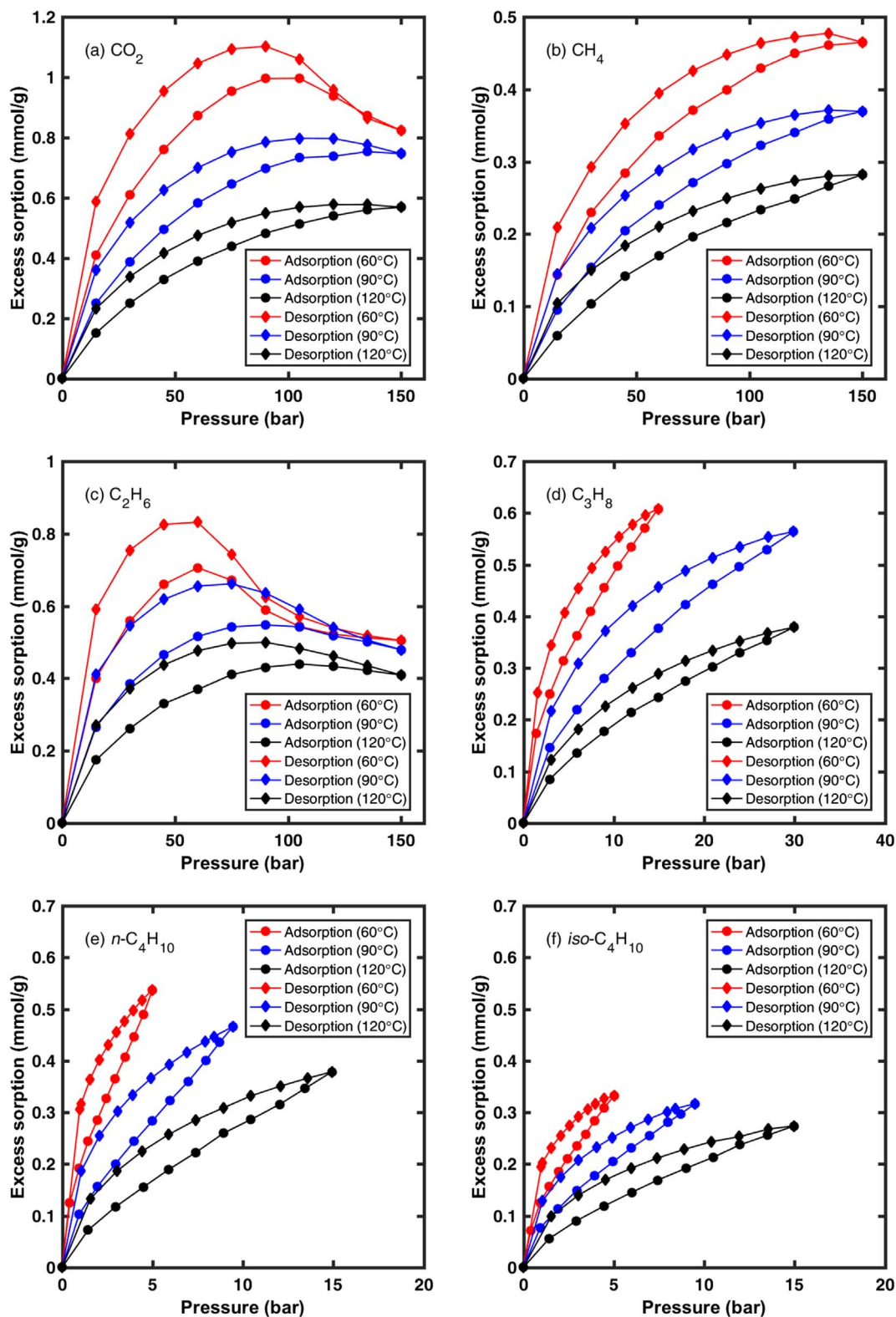$$F_A = (m^{SC} + m^{S} + m^{A})g \tag{1}$$

Fig. 3. Excess sorption isotherms of various hydrocarbons and carbon dioxide in Kimmeridge Blackstone at three different temperatures.

$$F_B = (V^{SC} + V^S + V^A)\rho g \qquad (2)$$

where m^A and V^A are the weight and volume of adsorbate, ρ is the density of the fluid and g is the gravity acceleration. Balance reading, Δm, and the mass of adsorbate m^A (that is, adsorbed mass) are

$$\Delta m = (F_A - F_B)/g = m^{SC} + m^S + m^A - (V^{SC} + V^S + V^A)\rho \qquad (3)$$

$$m^A = \Delta m - m^{SC} - m^S + (V^{SC} + V^S + V^A)\rho \qquad (4)$$

Density of the fluid is determined by a sinker, which has known weight and volume and m^{SC}, V^{SC}, m^S and V^S are measured in the blank measurement and buoyancy measurement. The only unknown is V^A, the volume of adsorbate. Volume of adsorbate may change during the adsorption and desorption. Excess sorption is reported based on the
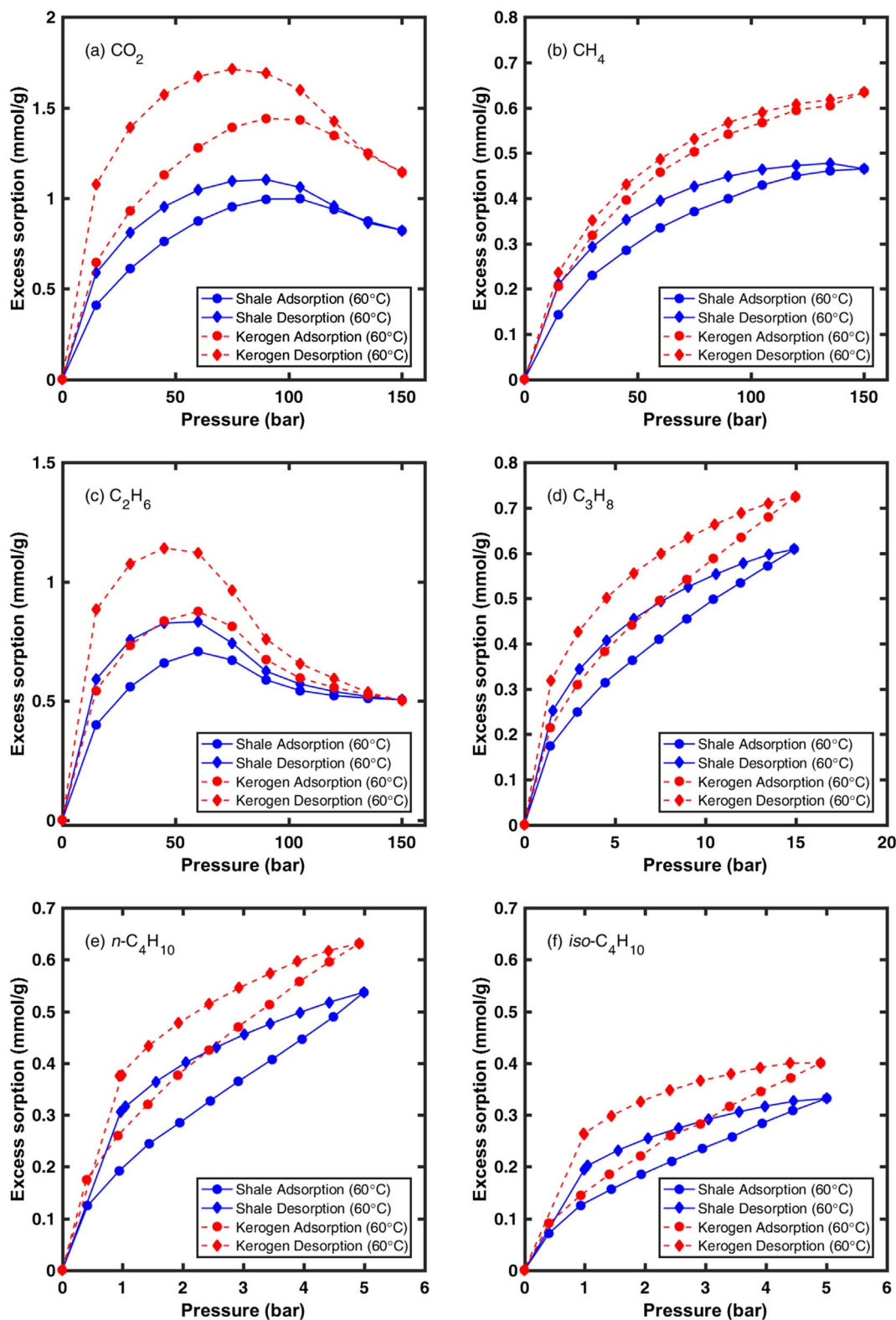
Fig. 4. Excess sorption isotherms of various hydrocarbons and carbon dioxide in Kimmeridge kerogen at 60 °C.

assumption that V^A is zero as:

$$m^{Excess} = \Delta m - m^{SC} - m^S + (V^{SC} + V^S)\rho \qquad (5)$$

We first report excess sorption defined above. In our data presentation, we divided m^A by the mass of the sample. Later we take into account the volume of the adsorbate and calculate the absolute adsorption. The calculated adsorption is based on two assumptions: 1)

there is no dissolution of gases in the kerogen, and 2) there is no swelling. We use two methods to compute the absolute adsorption. Many authors have used the density of a liquid to approximate the adsorbed layer density. One may also use the adsorbed layer density based on molecular simulations. In this work, we will examine the difference between the two and come up with specific suggestions. The absolute adsorption is related to the excess sorption by,

Table 5
Liquid density for absolute adsorption calculation.

Gas	Liquid			GCMC Simulation			
	Pressure (bar)	Temperature (°C)	Liquid density (kg/m³)	Pressure (bar)	Adsorbed layer density (kg/m³) (at 60 °C)	Adsorbed layer density (kg/m³) (at 90 °C)	Adsorbed layer density (kg/m³) (at 120 °C)
CH_4	1.01325	−161.48	422.36	150	279.41	248.95	224.30
C_2H_6	1.01325	−88.58	543.83	150	527.38	492.76	463.00
C_3H_8	1.01325	−42.11	580.88	15	474.25	–	–
$n-C_4H_{10}$	1.01325	−0.49	601.26	5	546.03	–	–
$iso-C_4H_{10}$	1.01325	−11.75	593.82	5	505.53	–	–
CO_2	5.1867	−56.56	1178.40	150	1123.43	994.20	871.04

$$m^{Absolute} = m^{Excess} + V^A \rho \tag{6}$$

$$V^A = \frac{m^{Absolute}}{\rho^{Ads}} \tag{7}$$

$$m^{Absolute} = m^{Excess} + \frac{m^{Absolute}}{\rho^{Ads}}\rho \tag{8}$$

$$m^{Absolute} = \frac{m^{Excess}}{1 - \rho/\rho^{Ads}} \tag{9}$$

where $m^{Absolute}$ and m^{Excess} represent absolute sorption and excess sorption, respectively. ρ^{Ads} is the average adsorbed layer density.

Adsorption is measured based on the equilibrium. For each of the measuring points, the pressure and temperature were in the range of setting pressure ± 0.1 bar and setting temperature ± 0.1 °C, respectively. If the weight change was smaller than the balance detection limit of 10 µg in five minutes with pressure and temperature in the range, we assumed that adsorption/desorption has reached the equilibrium. However, for the supercritical ethane and carbon dioxide adsorption, we set the weight change as high as 200 µg to avoid significant weight change by pressure fluctuation. For the methane adsorption, the equilibrium at each point was reached in about 0.5–1.5 h based on the above criteria. For the ethane and carbon dioxide adsorptions, it took 1–2.5 h to reach equilibrium at every set point. Each point in propane, n-butane and iso-butane adsorption took 1–2 h to reach equilibrium. It took longer to reach equilibrium at higher pressure.

On the desorption side, the equilibrium took longer to be established at each point. The time to reach equilibrium may vary in different adsorbents and adsorbates [11]. In this study, it took 2 h at most points. Only for the supercritical ethane and carbon dioxide, desorption the time was set to as high as 3 h. Pressure decrease in the desorption measurements was set as low as 2 bar/min, so the system pressure reached the range of setting pressure ± 0.1 bar in a few minutes. Major weight change of the sample occurred in this window. In desorption measurements of propane, n-butane, and iso-butane, the system temperature could be in the range of setting temperature ± 0.1 °C in a short time. However, for the supercritical ethane and carbon dioxide, the system temperature took 1–1.5 h to be in the range of setting temperature ± 0.1 °C. During this period, sample weight changed slightly mainly because of the temperature change. Once the pressure and temperature were in the range of setting pressure ± 0.1 bar and setting temperature ± 0.1 °C, the weight change of the sample was smaller than the balance detection limit in five minutes in most cases.

2.4. Molecular simulations

In this work, we use grand canonical Monte Carlo (GCMC) simulations to calculate hydrocarbon and CO_2 density profiles in nanopores including the adsorbed layer. In grand canonical ensemble, the chemical potentials μ of fluids, system volume V and temperature T are fixed. The number of molecules in the nanopores fluctuates throughout the simulation. The ensemble averaged number of molecules is fully determined by the chemical potentials.

We used the united atom model to simulate ethane, propane, n-butane, and iso-butane, and methane was treated as a single particle [12]. Non-bonded site-site interactions between groups on different molecules and groups belonging to the same molecule separated by more than three bonds are described by the modified Buckingham exponential-6 intermolecular potential [13]. The pairwise interaction potential $U(r)$ is given by:

$$U(r) = \begin{cases} \frac{\varepsilon}{1-\frac{6}{\alpha}}\left[\frac{6}{\alpha}\exp\left(\alpha\left[1-\frac{r}{r_m}\right]\right)-\left(\frac{r_m}{r}\right)^6\right], & r > r_{max} \\ \infty, & r < r_{max} \end{cases} \tag{10}$$

in which ε, r_m, and α are exponential-6 parameters. The variable r_m is the radial distance at which $U(r)$ reaches a minimum, and the cutoff distance r_{max} represents the smallest radial distance for which $dU(r)/dr = 0$ (Singh, 2009). The cutoff distance is required to avoid the original Buckingham exponential-6 potential become negative at very short distances [13]. The parameters ε, σ and α are 129.63 K, 0.3679 nm, and 16, respectively, for the CH_3 group; and 160.3 K, 0.373 nm, 15, respectively, for CH_4. For propane, n-butane, and iso-butane, the non-bonded interactions are described by the Lennard-Jones 12–6 model. The parameters ε/k_B and σ are 98 K, 0.375 nm, respectively, for the CH_3 group; 46 K, 0.395 nm, respectively, for the CH_2 group; and 10 K, 0.468 nm, respectively, for the CH group. The following combining rules are used to determine the cross parameters [14]:

$$\sigma_{ij} = \frac{1}{2}(\sigma_i + \sigma_j) \tag{11}$$

$$\varepsilon_{ij} = (\varepsilon_i\varepsilon_j)^{1/2} \tag{12}$$

$$\alpha_{ij} = (\alpha_i\alpha_j)^{1/2} \tag{13}$$

The bonded interactions of propane and butanes are described by the TraPPE model [12]. The bond lengths CH_3-CH_3, CH_3-CH_2, CH_2-CH_2, and CH_3-CH are 0.1540 nm, 0.1687 nm, 0.1535 nm, and 0.1540 nm, respectively. The bond bending potential is given as [15]:

$$U_{bend}(\theta) = \frac{K_\theta}{2}(\theta - \theta_{eq})^2 \tag{14}$$

where $K_\theta = 520$ kJ/mol/rad² and $\theta_{eq} = 114°$ for propane and n-butane [12], and $K_\theta = 520$ kJ/mol/rad² and $\theta_{eq} = 112°$ for iso-butane [16]. Torsion energy is given as [17]:

$$U_{tor}(\varphi) = V_0 + \frac{V_1}{2}(1 + \cos\varphi) + \frac{V_2}{2}(1-\cos2\varphi) + \frac{V_3}{2}(1 + \cos3\varphi) \tag{15}$$

where $V_0 = 0$, $V_1 = 355.03$ K, $V_2 = -68.19$ K, and $V_3 = 791.32$ K.

The potential model used for CO_2 molecules is from the flexible three-site EPM2 model, which includes the bond bending potential, the short-range LJ potential, and the long-range Coulomb potential [18]. The bond bending potential U_{bend} of each CO_2 molecule is given by Eq. (14) where $K_\theta = 1236$ kJ/mol/rad² and $\theta_{eq} = 180°$ [18]. The pairwise additive Lennard-Jones and Coulomb potentials are used to compute the CO_2-CO_2 interactions:
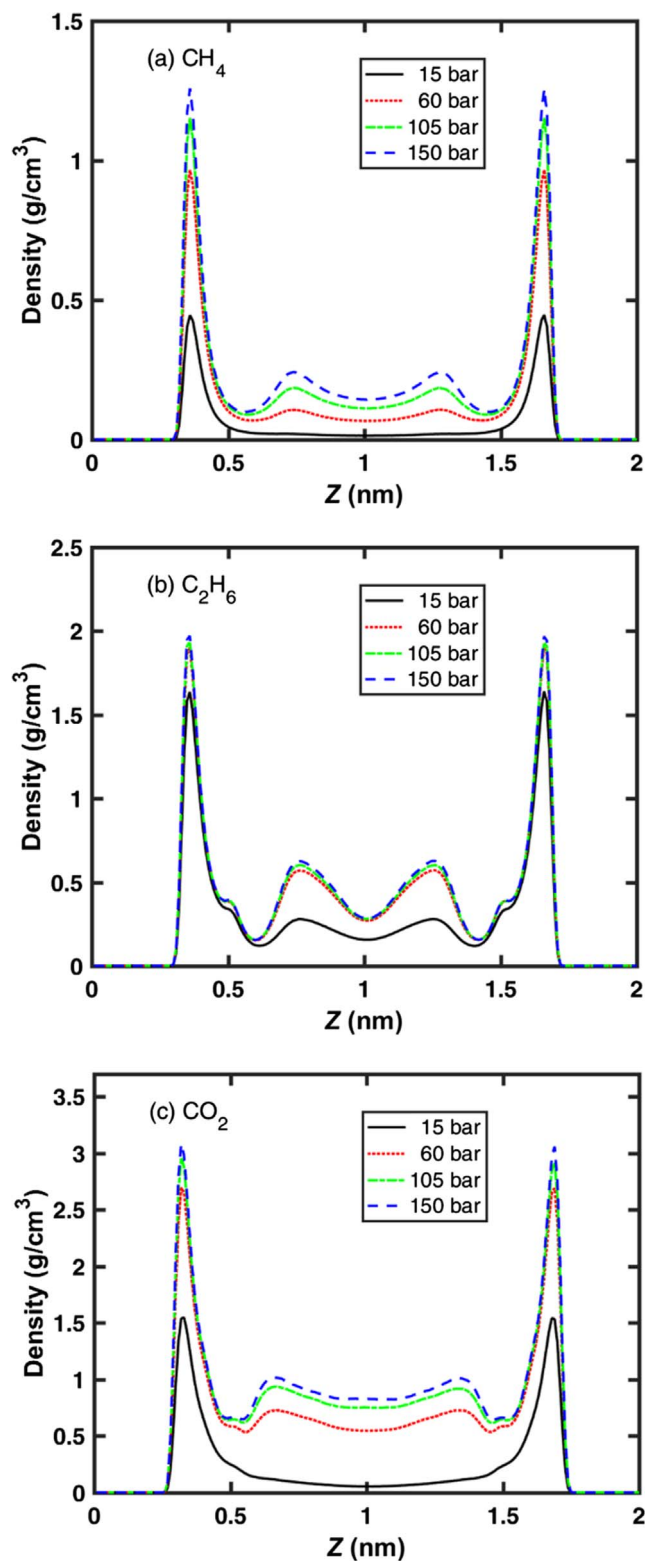
Fig. 5. Density distribution of CH$_4$, C$_2$H$_6$, and CO$_2$ adsorbed layer at various pressures near the solid surface at 60 °C from GCMC simulations. The slit pore width is 2 nm.

Fig. 6. Absolute adsorption of methane in Kimmeridge Blackstone at three different temperatures.

$$U(r_{ij}) = 4\varepsilon_{ij}\left[\left(\frac{\sigma_{ij}}{r_{ij}}\right)^{12} - \left(\frac{\sigma_{ij}}{r_{ij}}\right)^{6}\right] + \frac{q_i q_j}{4\pi\varepsilon_0 r_{ij}} \tag{16}$$

in which q_i is the partial charge of the site. The parameters q, ε and σ are 0.6512 e, 28.129 K and 0.2757 nm, respectively, for C; and -0.3256 e, 80.507 K and 0.3033 nm, respectively, for O. The conventional Lorentz-
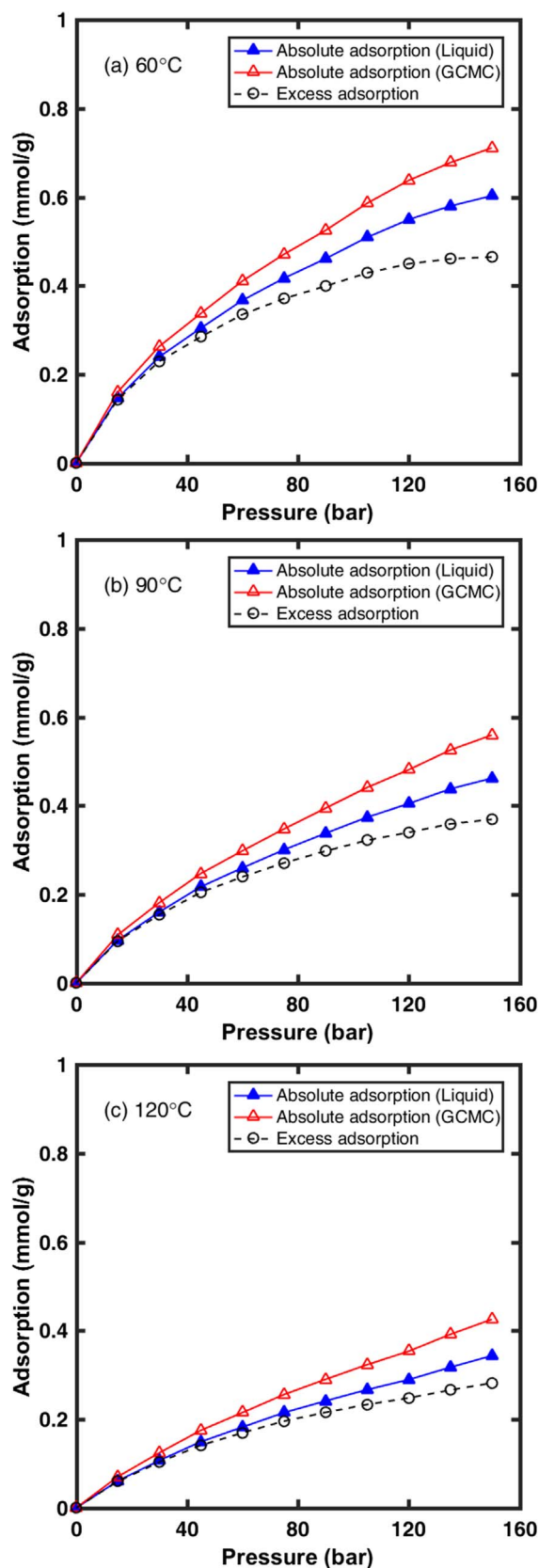
Berthelot combining rules are applied to the LJ parameters. The cutoff distance for CO$_2$ interaction is set to 1.07 nm.

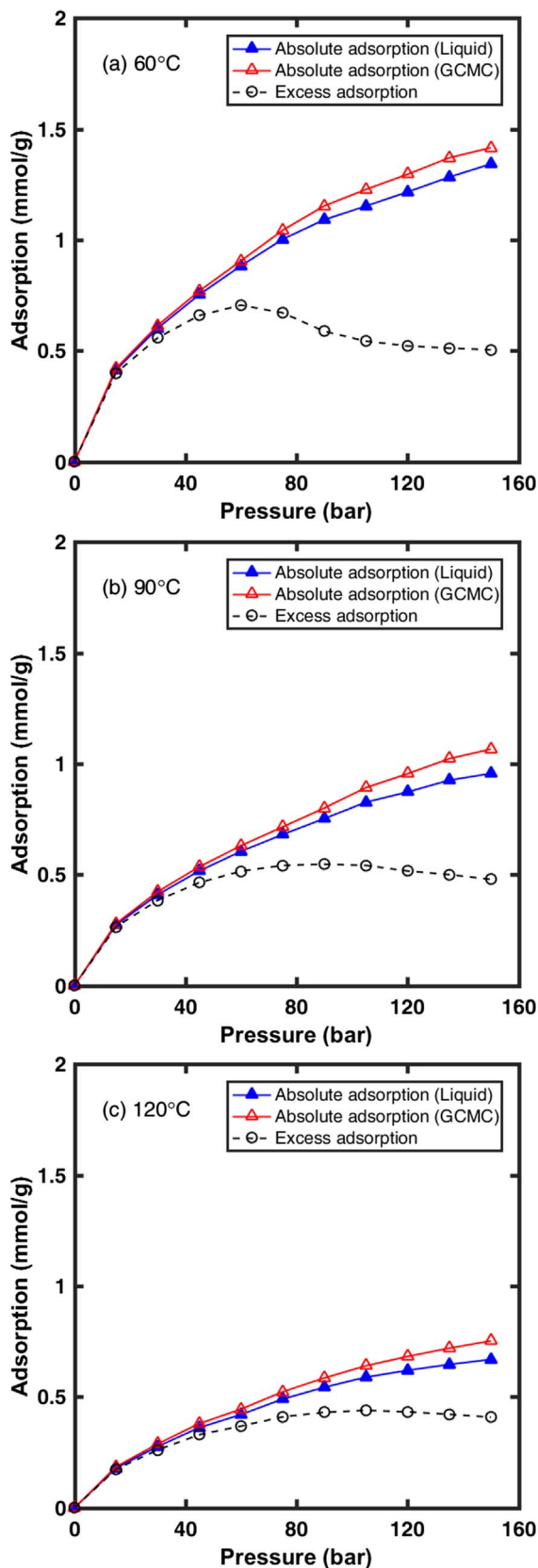In this work, pores were of slit geometry with smooth and

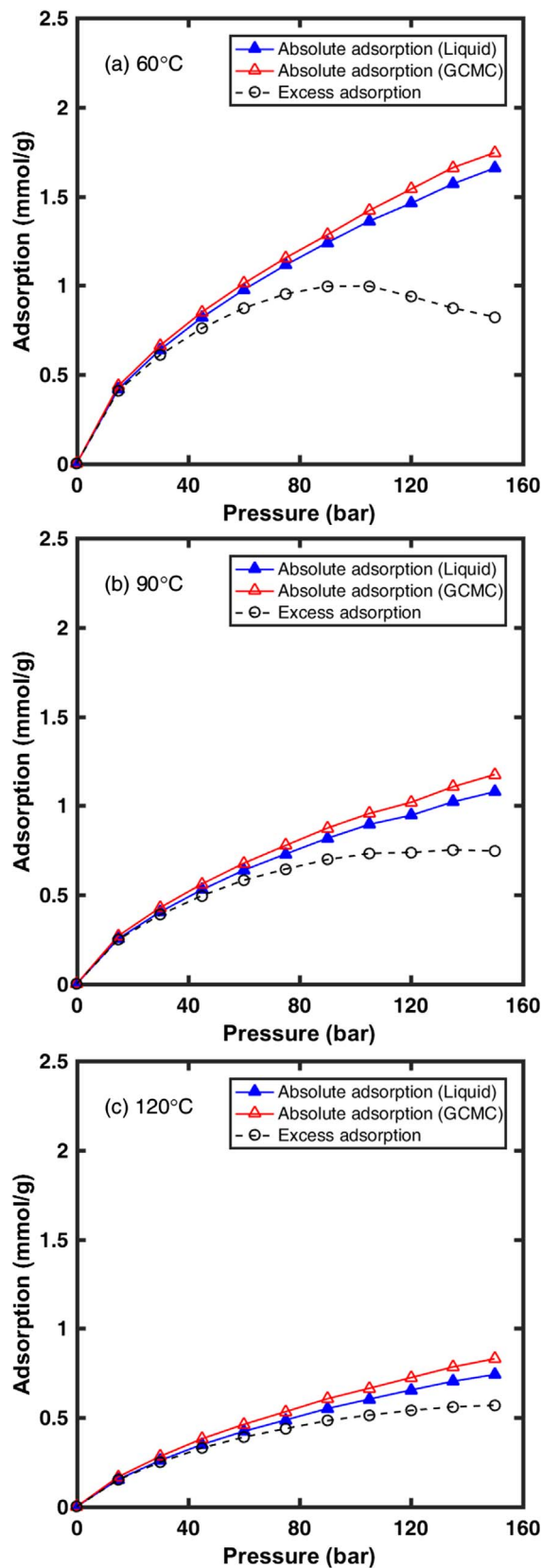**Fig. 7.** Absolute adsorption of ethane in Kimmeridge Blackstone at three different temperatures.

Fig. 8. Absolute adsorption of CO_2 in Kimmeridge Blackstone at three different temperatures.
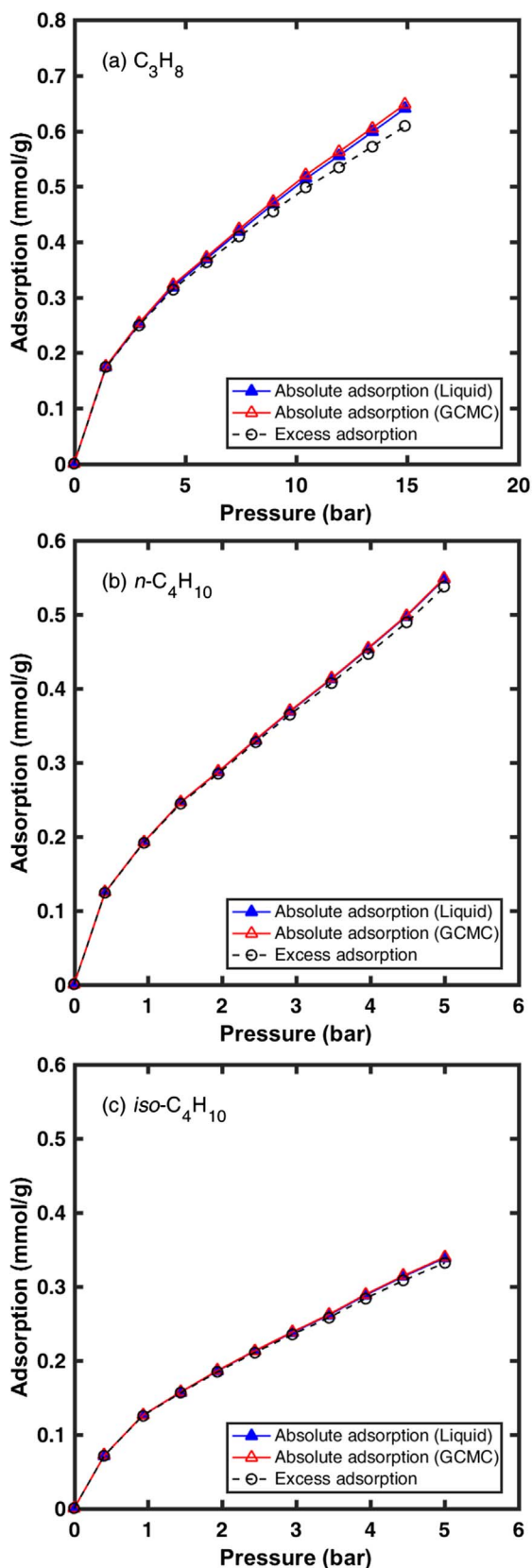
Fig. 9. Absolute adsorption of propane (a), *n*-butane (b) and *iso*-butane (c) in Kimmeridge Blackstone at 60 °C.

structureless carbon surfaces. We used 10-4-3 Steele potentials to describe the fluid-wall interaction φ_{wf} [19],

$$\varphi_{wf}(z) = 2\pi\rho_w\varepsilon_{wf}\sigma_{wf}^2\Delta\left[\frac{2}{5}\left(\frac{\sigma_{wf}}{z}\right)^{10} - \left(\frac{\sigma_{wf}}{z}\right)^4 - \frac{\sigma_{wf}^4}{3\Delta(0.61\Delta + z)^3}\right] \qquad (17)$$

where $\rho_w = 114\,\text{nm}^{-3}$, $\varepsilon_w = 28\,\text{K}$, $\sigma_w = 0.3345\,\text{nm}$, and $\Delta = 0.335\,\text{nm}$, respectively; the indices w and wf denote the wall and wall-fluid interactions, respectively. The combining rules based on Eqs. (11) and (12) are used to determine the cross parameters. The external potential Ψ in a slit pore is expressed as

$$\Psi(z) = \varphi_{wf}(z) + \varphi_{wf}(W-z) \qquad (18)$$

where W is the slit-pore size.

3. Results and discussion

3.1. Basic properties

The mineralogy of the inorganic part of Kimmeridge Blackstone is dominated by quartz, calcite and clay (Table 1). The thermal maturity in terms of vitrinite reflectance is 0.99% which is in the heart of the oil window.

Surface area, pore volume, and average pore size of Kimmeridge Blackstone and isolated kerogen powder samples were determined by nitrogen adsorption/desorption at −195.85 °C (77.3 K). Surface area was calculated using the Brunauer–Emmett–Teller (BET) model, while pore volume and average pore size was calculated by the Barrett–Joyner–Halenda (BJH) model. Fig. 2 shows the nitrogen adsorption/desorption of Kimmeridge Blackstone and isolated kerogen at −195.85 °C (77.3 K). The pore size distribution based on the adsorption isotherm is presented in Fig. S1.

As summarized in Table 2, the BET surface area of Kimmeridge Blackstone powders is 8.304 m²/g; the BJH pore volume of Kimmeridge Blackstone is 0.0336 cm³/g; Kimmeridge Blackstone sample has an average pore size of 18.5 nm. The average pore size of the isolated kerogen powder sample from Kimmeridge Blackstone is about 26 nm which is higher than Kimmeridge Blackstone sample. The BET surface area of the isolated Kimmeridge kerogen is 6.568 m²/g, which is slightly lower than the Kimmeridge Blackstone. However, the BJH pore volume of the isolated Kimmeridge kerogen is similar to the corresponding Kimmeridge Blackstone sample.

Table 3 shows the CHNS-O elemental analysis. Total carbon (organic and inorganic carbon) and total organic carbon (TOC) contents of shale samples were measured as well. The TOC in Kimmeridge Blackstone is above 50 wt%, while it is more than 60 wt% in the isolated kerogen. Because of the technique we used for kerogen isolation, the kerogen sample contains pyrite as an impurity, which results in the high content of sulfur. The Qualitative X-ray Diffraction (XRD) Analysis of the sample shows the evidence. Sample was scanned from 10 to 80° (2θ). The XRD plot of isolated Kimmeridge kerogen shows identical pyrite XRD patterns. If the isolated kerogen was pure, there should be no discernible peak from the powder XRD analysis.

From the CHNS-O elemental analysis in Table 3, hydrogen to carbon atom ratio is 1.246 and oxygen to carbon atom ratio is 0.067 in the isolated Kimmeridge kerogen which can be classified as Type II [20]. From the organic petrography analysis (Table 4), however, Kimmeridge Blackstone is interpreted to be of marine origin because of abundant fluorescing liptinite maceral in the form of lamalginite, degraded lamalginite and amorphinite. Trace amounts of inertinite maceral are observed in Kimmeridge Blackstone. Infrared spectroscopy (IR) analysis shows that aliphatic/aromatic ratio in Kimmeridge Blackstone is 9.98.

3.2. Sorption measurement

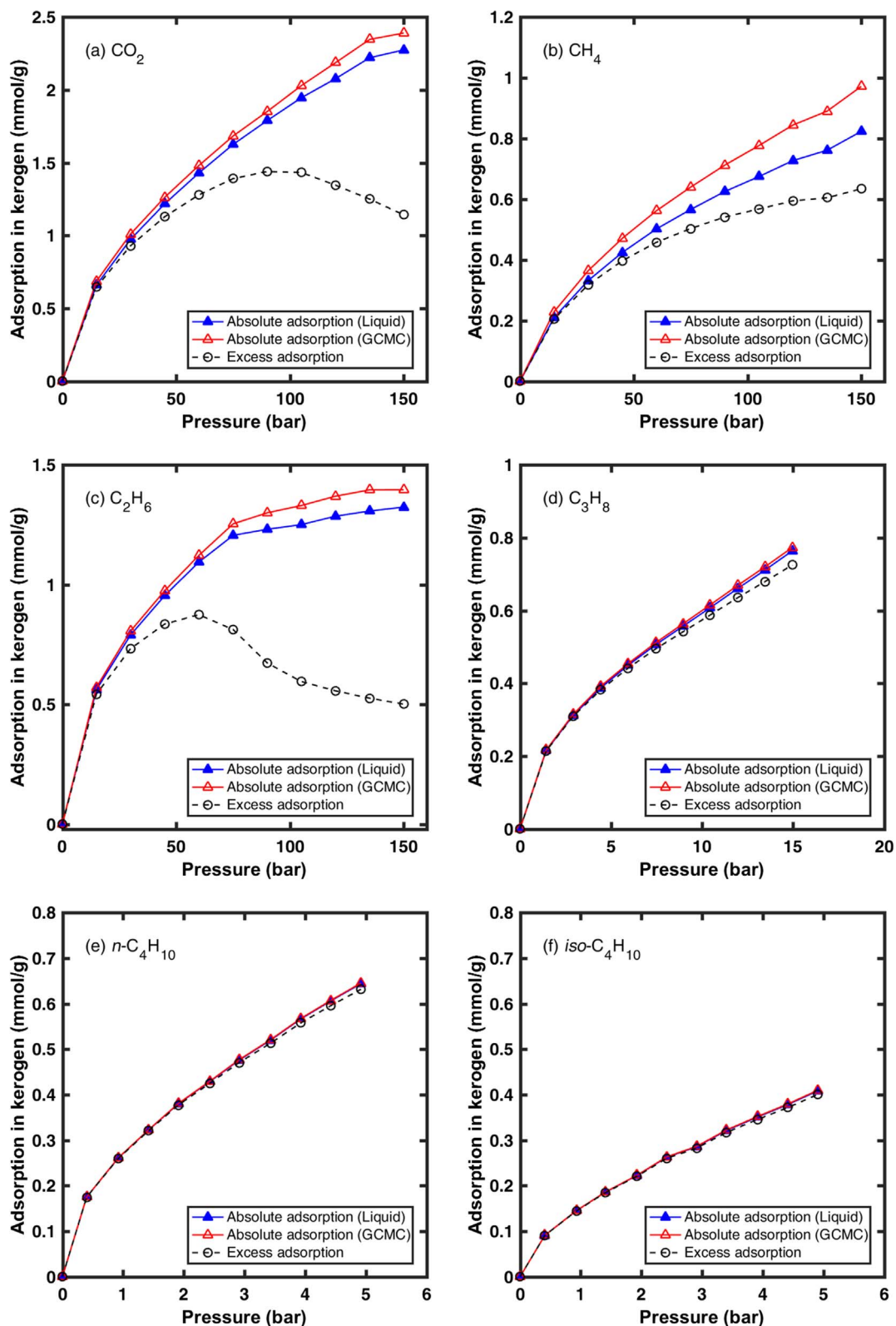Before sorption measurements, the density of Kimmeridge

Fig. 10. Absolute adsorption of CO_2 and various hydrocarbons in Kimmeridge kerogen at 60 °C.

Blackstone and the isolated kerogen samples was measured by helium gas at 60 °C. The densities of Kimmeridge Blackstone and Kimmeridge kerogen at 60 °C are 1.437 g/cm^3 and 1.318 g/cm^3, respectively (Table S1). In our previous work [6], the measured densities were slightly higher [6]. In this study, the samples were pretreated at 200 °C instead of 110 °C. Moreover, the shale powder samples are heterogeneous.

3.2.1. Excess sorption

Fig. 3 shows the excess sorption of various gases in Kimmeridge Blackstone at three different temperatures. The excess sorption is based on Eq. (5). The measurements are reproducible as can be seen in the results from duplicated experiments in Figs. S2–S4. The results reveal significant hysteresis. Compared with low pressure sorption in

Kimmeridge Blackstone presented in our recent work [6], the high pressure sorption shows more pronounced hysteresis, even for methane. This may be related to the reversible structure change during the sorption experiments, the capillary condensation, or the difference between the location of adsorbed and desorbed molecules in a given pore.

The excess sorption of methane is around 1/3 of carbon dioxide by mole (1/8 by mass) in line with literature data, and the excess sorption of ethane is close to carbon dioxide excess sorption in low pressure range (lower than 45 bar). *n*-butane has the highest adsorption at the same pressure and temperature conditions compared to all the other gases. As the temperature increases, the excess sorption decreases as expected.

At high pressure, the excess adsorption of ethane and carbon dioxide decreases as pressure increases. Generally, both the bulk fluid density and the adsorbed layer density will increase monotonically with the pressure increase. Because the density increase in the adsorbed layer may be lower than the increase in density of the bulk at high pressure, the excess adsorption may have a decreasing trend. On the other hand, for the supercritical methane and gaseous propane, *n*-butane, and *iso*-butane, the bulk density change is not significant enough at the experimental condition in this work, so there is no pronounced decrease in the excess adsorption. For *n*-butane and *iso*-butane, although they have the same molecular weight, the excess adsorption is different significantly, which can be as high as 55%.

Fig. 4 shows the excess sorption of various gases in the isolated Kimmeridge kerogen at 60 °C. We have also included the data for the corresponding Blackstone shale powders for the purpose of comparison. The results show that Kimmeridge kerogen has higher excess sorption than Kimmeridge shale sample. The sorption of light hydrocarbon and carbon dioxide is a strong function of kerogen content. The excess sorption isotherms in isolated kerogens have similar shape as in their corresponding shale sample.

3.2.2. Absolute adsorption

The absolute adsorption can be calculated from excess adsorption based on Eq. (9) with knowledge of bulk density and adsorbed layer density. In this work, the liquid density and the estimated adsorbed layer density from GCMC simulations in slit pores are used to examine the difference. The liquid densities in Table 5 [21] are at atmospheric pressure at the boiling point of hydrocarbons and at the triple point of carbon dioxide. The GCMC simulations were conducted in three different pore sizes (e.g. 2 nm, 5 nm, and 10 nm slit pores) for methane, ethane and carbon dioxide at temperatures corresponding to the experiments. The density profiles of methane, ethane and carbon dioxide in the 2-nm slit pores at 60 °C are presented in Fig. 5. The rest are presented in Figs. S5–S7. The results indicate that the monolayer adsorption is pronounced at relatively low pressure and the second adsorbed layer develops at relatively high pressure. The positions of the peaks of the first two layers are the same for the same gas in the same pore at different pressures and temperatures. The average adsorbed layer densities are calculated based on the average within specified regions based on different assumptions. Two regions were defined in this work (Fig. S8). Region A is from the center of the structureless carbon, which is the position of $z = 0$ for the 10-4-3 Steele potential model in Eq. (17), to the peak of the second adsorbed layer. Region B is the area between the first two peaks of the adsorbed layer. The results show that the average adsorbed layer density from Region A is lower than that from Region B (Fig. S9), because Region A has a blank area due to the strong repulsion near the wall. It is reasonable to use the value from Region B based on the straightforward definition of adsorbed layer. The results indicate that the adsorbed layer density is nearly independent of pore sizes (Fig. S9). The calculated absolute adsorptions of methane, ethane and carbon dioxide at different temperatures, based on liquid density assumption and estimated value from GCMC simulations, are presented in Figs. 6–8, respectively. The

corresponding excess adsorptions are also included for comparison. For the three gases, the absolute adsorptions increase monotonically with pressure increase. The absolute adsorption of methane shows significant difference based on the liquid density and the adsorbed layer density; they are almost the same for ethane and carbon dioxide. The main reason is that the liquid density of methane is not well defined at temperatures of 60, 90, and 120 °C. The adsorbed layer density of methane from GCMC simulations has a clear foundation.

For propane, *n*-butane and *iso*-butane, the GCMC simulations were performed at 60 °C. The average adsorbed layer densities were calculated based on the same method as the other three gases (Fig. 9). The absolute adsorption was calculated based on two different adsorbed layer densities, as well. The results show that the absolute adsorption is very close to the excess adsorption due to the significantly higher adsorbed layer density than the bulk phase. The absolute adsorption can be approximated by the excess adsorption. The plots in Figs. S10 and S11 show that, although the two butanes have the same molecular weight and the same bulk densities, the adsorption is likely affected by the molecular shape and orientation. The difference of the adsorbed layer density from simulations is not as pronounced as the difference of excess adsorption of *n*-butane and *iso*-butane from experiments (Figs. 9 and S12). The pore surface in shale is not smooth, and may provide more adsorption sites and have more significant effect on the molecules' orientation.

The absolute adsorption in Kimmeridge kerogen at 60 °C is presented in Fig. 10. The adsorption isotherms in isolated kerogens have similar shape as in their corresponding shale sample as well, which implies that the adsorption in kerogen may be dominant in the shale sample.

4. Conclusions

The main conclusions drawn from this work are:

1. There is significant hysteresis in sorption at high pressure for all the fluids even for methane, which may be related to the reversible structure change during the sorption measurements, and capillary condensation.
2. At the temperature and pressure conditions in this work, the absolute adsorption increases monotonically with pressure as expected.
3. The absolute adsorption based on liquid density and GCMC simulations are close except for methane. The liquid density of methane is not well defined for the conditions in shale media.
4. For propane, *n*-butane, and *iso*-butane, the absolute adsorption plots are very close to the excess adsorption to the pressure conditions where these species are gas.
5. For the isolated kerogen, both the excess adsorption and the absolute adsorption have the similar shape as in their corresponding Blackstone, implying that the adsorption in kerogen may be dominated in the shale sample.
6. For *n*-butane and *iso*-butane, although they have the same molecular weight and similar bulk liquid densities, the excess adsorption and absolute adsorption are significantly different. The density of the *n*-butane adsorbed layer from molecular simulations is about 10% higher than *iso*-butane on molecularly smooth surfaces. Molecular simulation of adsorption on non-smooth surfaces may be required to get further insight.

All the adsorption results presented in this work were based on the assumption of no dissolution and no swelling in the samples. Indications are that these assumptions are valid in the shale used in this work.

We also like to emphasize that ρ^{Ads} is the key parameter in the absolute adsorption used in this work. A different approach is the use of Eq. (6) which requires the estimation of adsorbed layer volume V^A. Direct estimation of V^A from excess adsorption will be the subject of a

future publication.

Acknowledgements

Appendix A. Supplementary data

Supplementary data associated with this article can be found, in the online version, at http://dx.doi.org/10.1016/j.fuel.2018.02.186.

References

[1] Gallois R. Oil shale resources in Great Britain. London: Institute of Geological Sciences; 1979. p. 2.

[2] Vandenbroucke M, Largeau C. Kerogen origin, evolution and structure. Org Geochem 2007;38(5):719–833.

[3] Li Z, Jin Z, Firoozabadi A. Phase behavior and adsorption of pure substances and mixtures and characterization in nanopore structures by density functional theory. SPE J 2014;19(06). 1,096-1,109.

[4] Jin Z, Firoozabadi A. Methane and carbon dioxide adsorption in clay-like slit pores by Monte Carlo simulations. Fluid Phase Equilib 2013;360:456–65.

[5] Etminan SR, Javadpour F, Maini BB, Chen Z. Measurement of gas storage processes in shale and of the molecular diffusion coefficient in kerogen. Int J Coal Geol 2014;123:10–9.

[6] Zhao H, Lai Z, Firoozabadi A. Sorption hysteresis of light hydrocarbons and carbon dioxide in shales and kerogens. Sci Rep 2017;7(1):16209.

[7] Gasparik M, Rexer TF, Aplin AC, Billemont P, De Weireld G, Gensterblum Y, et al. First international inter-laboratory comparison of high-pressure CH4, CO2 and C2H6 sorption isotherms on carbonaceous shales. Int J Coal Geol 2014;132:131–46.

[8] Yuan W, Pan Z, Li X, Yang Y, Zhao C, Connell LD, et al. Experimental study and modelling of methane adsorption and diffusion in shale. Fuel 2014;117(Part A):509–19.

[9] Wang K, Wang G, Ren T, Cheng Y. Methane and CO2 sorption hysteresis on coal: a critical review. Int J Coal Geol 2014;132:60–80.

[10] Horvath Z, Jackson K. Procedure for the Isolation of Kerogen from Sedimentary Rocks. Bureau of Mineral Resources, Geology and Geophysics; 1981.

[11] Kelemen S, Kwiatek L, Siskin M, Lee A. Structural response of coal to drying and pentane sorption. Energy Fuels 2006;20(1):205–13.

[12] Martin MG, Siepmann JI. Transferable potentials for phase equilibria. 1. United-atom description of n-alkanes. J Phys Chem B 1998;102(14):2569–77.

[13] Errington JR, Panagiotopoulos AZ. A new intermolecular potential model for the n-alkane homologous series. J Phys Chem B 1999;103(30):6314–22.

[14] Singh SK, Sinha A, Deo G, Singh JK. Vapor−liquid phase coexistence, critical properties, and surface tension of confined alkanes. J Phys Chem C 2009;113(17):7170–80.

[15] Van der Ploeg P, Berendsen H. Molecular dynamics simulation of a bilayer membrane. J Chem Phys 1982;76(6):3271–6.

[16] Martin MG, Siepmann JI. Novel configurational-bias Monte Carlo method for branched molecules. Transferable potentials for phase equilibria. 2. United-atom description of branched alkanes. J Phys Chem B 1999;103(21):4508–17.

[17] Smit B, Karaborni S, Siepmann JI. Computer simulations of vapor–liquid phase equilibria of n-alkanes. J Chem Phys 1995;102(5):2126–40.

[18] Harris JG, Yung KH. Carbon dioxide's liquid-vapor coexistence curve and critical properties as predicted by a simple molecular model. J Phys Chem 1995;99(31):12021–4.

[19] Steele WA. The physical interaction of gases with crystalline solids: I. Gas-solid energies and properties of isolated adsorbed atoms. Surf Sci 1973;36(1):317–52.

[20] Peters KE, Walters CC, Moldowan JM. The biomarker guide. 2nd ed. Cambridge: Cambridge University Press; 2005.

[21] Linstrom P, Mallard W. NIST chemistry webbook; NIST standard reference database No. 69; 2010. http://webbook.nist.gov/chemistry/.